nature communications

Article

https://doi.org/10.1038/s41467-024-52104-z

Tuning the fluidity and protein corona of ultrasound-responsive liposomal nanovaccines to program T cell immunity in mice

Received: 15 August 2023

Accepted: 27 August 2024

Published online: 16 September 2024

Check for updates

Jia He[1,2], Chaoyu Wang[1,2], Xiao Fang[1,2], Junyao Li[1,2], Xueying Shen[1,2], Junxia Zhang[2,3,4], Cheng Peng[2,3,4], Hongjian Li[5], Sai Li[2,3,4], Jeffrey M. Karp[6,7,8,9] & Rui Kuai[1,2]

Inducing high levels of antigen-specific CD8α$^+$ T cells in the tumor is beneficial for cancer immunotherapy, but achieving this in a safe and effective manner remains challenging. Here, we have developed a designer liposomal nanovaccine containing a sonosensitizer (LNVS) to efficiently program T cell immunity in mice. Following intravenous injection, LNVS accumulates in the spleen in a protein corona and fluidity-dependent manner, leading to greater frequencies of antigen-specific CD8α$^+$ T cells than soluble vaccines (the mixture of antigens and adjuvants). Meanwhile, some LNVS passively accumulates in the tumor, where it responds to ultrasound (US) to increase the levels of chemokines and adhesion molecules that are beneficial for recruiting CD8α$^+$ T cells to the tumor. LNVS + US induces higher levels of intratumoral antitumor T cells than traditional sonodynamic therapy, regresses established mouse MC38 tumors and orthotopic cervical cancer, and protects cured mice from relapse. Our platform sheds light on the importance of tuning the fluidity and protein corona of naovaccines to program T cell immunity in mice and may inspire new strategies for cancer immunotherapy.

Increasing evidence has shown that the levels of tumor antigen-specific CD8α$^+$ T cells are positively correlated with the prognosis of cancer patients[1–3]. This has motivated a variety of strategies that can increase the levels of intratumoral CD8α$^+$ T cells. Among these strategies, peptide cancer vaccines have been widely used to enhance CD8α$^+$ T cell responses due to their good safety and ease of manufacturing[4–7]. This is typically achieved by delivering cancer vaccines to lymphoid organs such as the lymph nodes, where antigen-presenting cells such as dendritic cells take up vaccines consisting of antigens and adjuvants, present antigen epitopes in the context of MHC class I, and upregulate costimulatory signals and cytokines. When naïve T cells receive these signals, they proliferate and circulate throughout the body to kill tumor cells[8,9]. While many cancer vaccines have been shown to expand tumor antigen-specific T cells efficiently, these T cells do not always efficiently reach the tumor[10,11], thus leading to suboptimal therapeutic efficacy[12]. Previous studies have shown that the administration of vaccines followed by the local administration of chemokines or TLR agonists can facilitate the recruitment of antigen-

[1]School of Pharmaceutical Sciences, Tsinghua University, Beijing, China. [2]Tsinghua-Peking Center for Life Sciences, Beijing, China. [3]School of Life Sciences, Tsinghua University, Beijing, China. [4]Frontier Research Center for Biological Structure & State Key Laboratory of Membrane Biology, Beijing, China. [5]School of Medicine, Tsinghua University, Beijing, China. [6]Department of Anesthesiology, Perioperative, and Pain Medicine, Brigham and Women's Hospital, Harvard Medical School, Boston, MA, USA. [7]Harvard-MIT Program in Health Sciences and Technology, MIT, Cambridge, MA, USA. [8]Harvard Stem Cell Institute, Harvard University, Cambridge, MA, USA. [9]Broad Institute of MIT and Harvard, Cambridge, MA, USA. e-mail: ruikuai@tsinghua.edu.cn

specific T cells to the target tissue[13–15], but they require intratumoral injection of chemokines or TLR agonists, which can be technically challenging for tumors that are hard to reach through direct injections.

An ideal solution is to design a peptide vaccine formulation which upon intravenous injection, can not only target lymphoid organs such as the spleen to expand T cells[16–18], but also can precisely modulate the tumor microenvironment to boost chemokine secretion and facilitate T cell recruitment. On the one hand, to target the spleen, incorporation of the helper lipid DOPA into LNP containing ionizable lipids[19–21] or incorporation of senescent red blood cell membrane into nanoparticles[22] have been shown to achieve spleen-targeted delivery, but the relatively complex lipid compositions may limit their wide use for peptide vaccine delivery and the ionizable lipid can cause potential toxicity at high doses[23]. On the other hand, to precisely modulate the tumor microenvironment, the vaccine formulation can be equipped with a sonosensitizer and delivered to the tumor so that it can respond to external ultrasound to generate reactive oxygen species (sonodynamic therapy) and boost chemokine secretion to recruit T cells[24,25]. Since ultrasound has easy access to different parts of the body, this strategy can be broadly applicable to different tumors[26]. However, how to develop a simple and safe vaccine formulation that can efficiently target the spleen and tumor for programming T cell immunity remains elusive.

Here, we show that liposomes accumulate in the spleen in a protein corona and fluidity-dependent manner. Liposomes with a complement C3-containing protein corona and high fluidity accumulate in the spleen efficiently. We further load the selected liposomes with lipidated antigen peptides, lipidated CpG, and sonosensitizer to obtain LNVS. Intravenously injected LNVS efficiently accumulates in the spleen to expand antigen-specific CD8α$^+$ T cells, and some passively accumulates in the tumor, where it responds to ultrasound and increases chemokines and adhesion molecules to enhance intratumoral T cell recruitment, leading to potent therapeutic effects on the MC38 tumor model and orthotopic cervical cancer model (Supplementary Fig. 1). Depleting circulating T cells or total CD8α$^+$ T cells significantly compromises the therapeutic effect of LNVS + US, indicating that CD8α$^+$ T cell recruitment to the tumor is critical for maximizing the therapeutic effect.

Results

Preparation and characterization of spleen-targeting liposome carriers

We first focused on several negatively or neutrally charged phospholipids such as 1,2-dioleoyl-sn-glycero-3-phosphate (DOPA), 1,2-dioleoyl-sn-glycero-3-phospho-L-serine (DOPS), 1,2-dioleoyl-sn-glycero-3-phospho-1′-rac-glycerol (DOPG), 1,2-dioleoyl-sn-glycero-3-phosphocholine (DOPC), and 1,2-dioleoyl-sn-glycero-3-phosphoethanolamine (DOPE), all of which share the same lipid tail, for preparing liposome carriers due to their excellent safety profiles and potential for targeting antigen-presenting cells that are highly phagocytic (Fig. 1a). The above five phospholipids-based liposome carriers were homogeneous and had a diameter around 150 nm (Fig. 1b). As expected, DOPA, DOPS, DOPG-based liposomes had a negative zeta potential, while DOPC and DOPE-based liposomes had a neutral zeta potential (Fig. 1c). We next analyzed the impact of phospholipids on the pharmacokinetics (PK) and biodistribution. All liposomes exhibited similar PK profiles (Supplementary Fig. 2), but DOPE-based liposomes exhibited up to 5.4-fold more efficient accumulation in the spleen than other phospholipids-based liposomes (Fig. 1d). DOPE-based liposomes had a spleen/liver ratio close to 2.5, significantly higher than other phospholipids-based liposomes whose spleen/liver ratios were below 1 ($P < 0.0001$, Fig. 1e). The spleen targeting of DOPE-based liposomes was similar when the phospholipid concentration was in the range of 2–6 mg/ml (Supplementary Fig. 3), making this platform a robust delivery system for cancer vaccines. Further analysis indicated that DOPE-based liposomes were more efficiently taken up by antigen-presenting cells such as macrophages and dendritic cells in the spleen compared with other phospholipids-based liposomes, which is beneficial for the activation of antigen-specific CD8α$^+$ T cell responses (Fig. 1f). CD11c$^+$ DC depletion compromised the spleen targeting of DOPE-liposomes, but cDC1 deficient (*Batf3*$^{-/-}$) mice exhibited a similar level of DOPE-liposomes in the spleen, probably because the number of cDC1 is too small to change the spleen accumulation profile (Supplementary Fig. 4).

To understand the mechanism underlying the excellent spleen targeting properties of DOPE-based liposomes, we incubated different types of liposomes with mouse plasma and analyzed the composition of protein corona on liposomes using mass spectrometry. The most abundant protein bound to DOPA-based liposomes was beta-2-glycoprotein 1, while the most abundant protein bound to DOPS, DOPG, and DOPC-based liposomes was albumin. Notably, DOPE-based liposomes had the most complement C3 bound to the surface, indicating that the complement C3 might be critical for the spleen targeting of DOPE-based liposomes (Fig. 1g). Interestingly, incubation of DOPE-liposomes with plasma from C3 KO female C57BL/6 led to the formation of a protein corona that not only lacks the complement C3 but also contains proteins that are absent in the case of DOPE-liposomes incubated with WT plasma (Supplementary Fig. 5). While the exact reason for this phenomenon is beyond the scope of this manuscript, we speculate that this may be caused by the interactions between the complement C3 and other proteins. To further confirm the role of the complement C3, we intravenously injected DOPE-based liposomes in WT female C57BL/6 mice or C3 KO female C57BL/6 mice and harvested major organs for ex vivo imaging at 6 h post injection. Notably, DOPE-based liposomes had 2-fold less accumulation in the spleen of C3 KO female C57BL/6 mice compared with that of WT female C57BL/6 mice ($P < 0.001$, Fig. 1h, i), indicating C3 was at least partially involved in mediating the spleen targeting of DOPE-based liposomes.

Preparation and characterization of liposomal nanovaccines (LNV)

To prepare DOPE-based LNV, ethanol containing DOPE, cholesterol, DOPE-PEG, and DOPE-antigen were mixed with DI water containing cholesterol-CpG and extruded through 400-nm polycarbonate membranes to obtain LNV. A similar protocol was used to prepare other phospholipids-based LNV using DOPA, DOPS, DOPG, and DOPC to replace DOPE. The above five phospholipids-based LNVs were homogeneous and had a diameter around 150 nm (Fig. 2a). All LNVs had a negative zeta potential due to the presence of negatively charged cholesterol-CpG (Fig. 2b). Regardless of the phospholipids used, the loading efficiency of antigen peptides and CpG in LNVs was over 90% and 82%, respectively (Supplementary Fig. 6). Cryo-electron microscopy (cryo-EM) confirmed the homogeneous size distribution of LNVs containing different phospholipids (Fig. 2c). To understand whether the presence of antigen peptides and CpG had any effect on the biodistribution profile, we intravenously injected DOPE-based liposomes or DOPE-based LNV into female C57BL/6 mice and harvested major organs for ex vivo imaging. As expected, loading antigens and CpG did not change the biodistribution profile (Supplementary Fig. 7). Interestingly, compared with other phospholipids-based LNV, DOPE-LNV induced stronger antigen presentation (Fig. 2d, e), which can be ascribed to the fusogenic properties of DOPE that can promote fusion with endosomal membrane and enhance the cross-presentation[27]. Further analysis indicated that macrophages and dendritic cells in the spleen were positive both for the antigens and liposomes (Supplementary Fig. 8). To understand the impact of phospholipids on the expansion of antigen-specific CD8α$^+$ T cells, we intravenously injected the above five phospholipids-based LNVs into naïve female C57BL/6 mice on days 0 and 5 and measured the frequency of antigen-specific CD8α$^+$ T cells on day 10 (Fig. 2f). DOPE-based LNV induced ~20% antigen-specific CD8α$^+$ T cells among peripheral blood mononuclear

https://doi.org/10.1038/s41467-024-52104-z

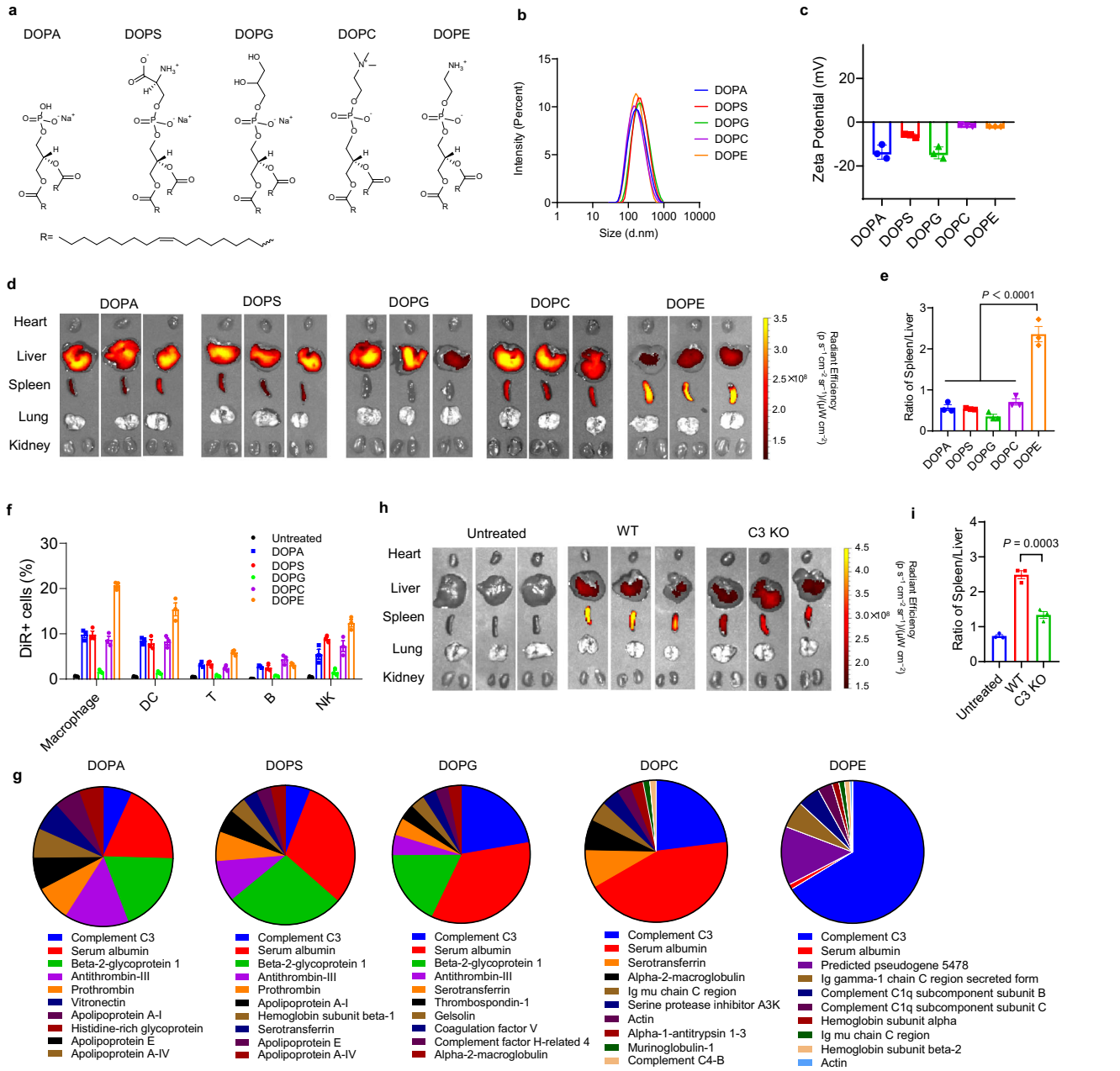

Fig. 1 | The biodistribution of liposomes is highly dependent on the protein corona. a Chemical structures of phospholipids used for the preparation of liposomes. The size distribution (**b**) and zeta potential (**c**) of liposomes prepared with indicated phospholipids ($n = 3$ experimental replicates per group). **d** The biodistribution of indicated liposome formulations in C57BL/6 mice at 6 h post intravenous injection. **e** The ratio of indicated liposome formulations in the spleen and liver at 6 h post intravenous injection ($n = 3$ mice per group). **f** The uptake of indicated liposome formulations by different subsets of immune cells in the spleen at 6 h post intravenous injection ($n = 3$ mice per group). **g** The composition of protein corona on liposomes prepared with indicated phospholipids. The data are representative of two independent experiments. **h** The biodistribution of DOPE liposomes in WT C57BL/6 and C3 KO C57BL/6 mice. **i** The ratio of DOPE liposomes in the spleen and liver at 6 h post intravenous injection in WT C57BL/6 and C3 KO C57BL/6 mice ($n = 3$ mice per group). Data were analyzed by one-way analysis of variance (ANOVA) with Tukey's multiple comparisons post-test. Data represent mean ± SEM.

cells (PBMCs), which was 10-fold stronger than the soluble vaccine ($P < 0.0001$) and 3 to 5-fold stronger than other phospholipids-based LNVs ($P < 0.0001$, Fig. 2g, h). DOPE-based LNV induced IFN-β levels in vivo at early time points (Supplementary Fig. 9a). DOPE-based LNV also induced higher levels of $CD69^+$ $CD8^+$T cells in the spleen and blood (Supplementary Fig. 9b–e). The percent of IFN-γ^+ $CD8^+$ T cells was 20.5% upon restimulation by the corresponding antigen used in the vaccine, indicating that the $CD8^+$ T cells were functional for cytokine production (Supplementary Fig. 10). DOPE-based LNV induced 3.5-fold weaker $CD8\alpha^+$ T cell responses in C3 KO mice than in WT mice ($P < 0.01$, Fig. 2i, j), further confirming that C3 plays an important role in mediating the T cell activation of DOPE-LNV[28].

We also performed additional experiments to understand the role of lymph nodes. Notably, the nanovaccine showed substantial accumulation in the spleen but not in the lymph nodes (Supplementary Fig. 11a), indicating the spleen may play a more important role in T cell priming than lymph nodes. Indeed, splenectomy (spleen depletion) significantly reduced the percent of antigen-specific T cells in the blood, while the percent of antigen-specific T cells in the lymph node was close to the background level for animals with or without the

https://doi.org/10.1038/s41467-024-52104-z

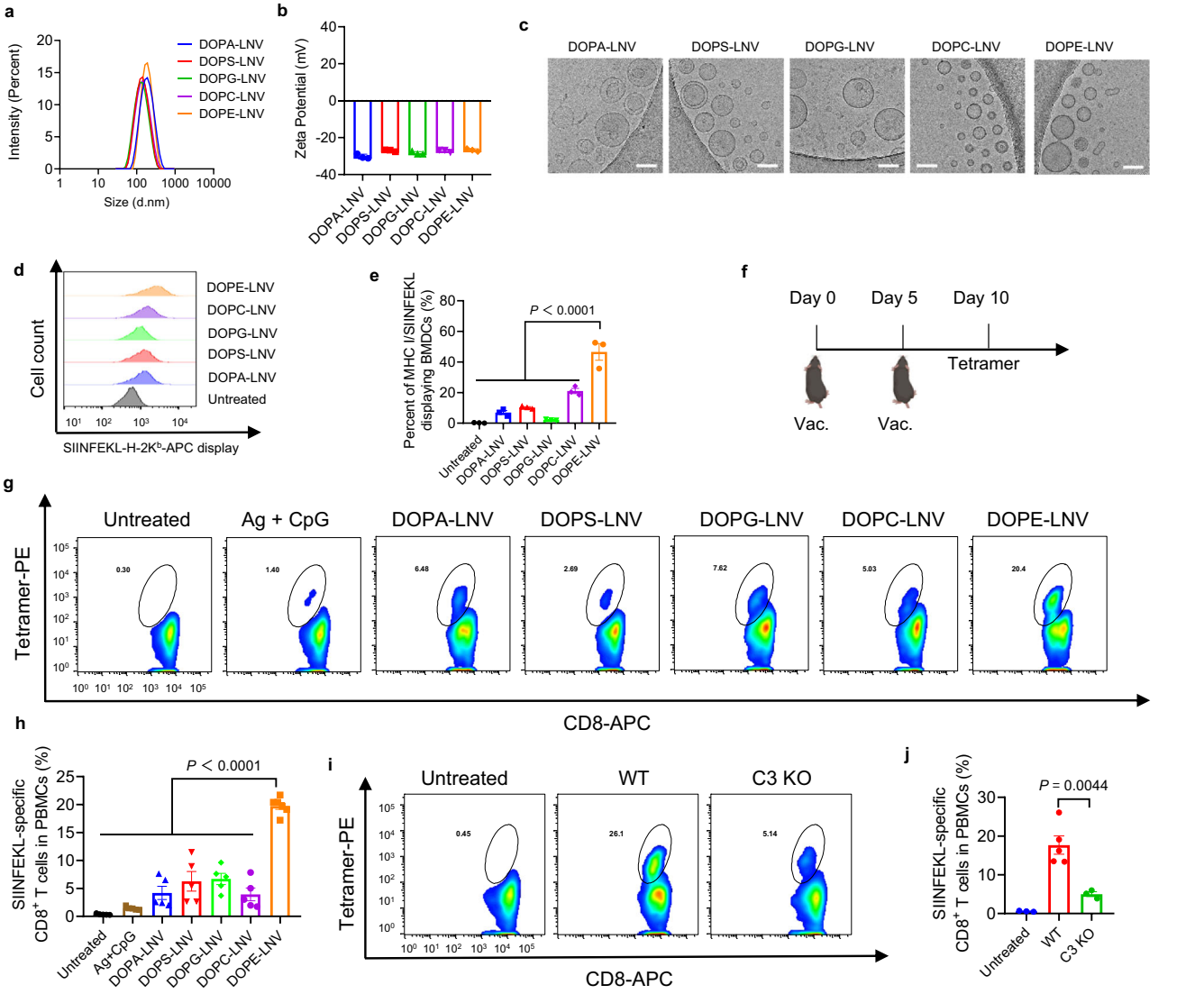

Fig. 2 | LNV induces antigen-specific T cell responses in a lipid composition-dependent manner. Size distribution (**a**) and zeta potential (**b**) of LNV prepared with indicated phospholipids ($n = 3$ experimental replicates per group). **c** Cryo-electron microscopy (cryo-EM) of LNV containing different phospholipids, scale bar = 100 nm. The data are representative of two independent experiments. BMDCs were treated with indicated formulations for 6 h, and the antigen presentation was measured using flow cytometry. Shown are representative histograms (**d**) and quantification of antigen presentation efficiency (**e**) ($n = 3$ experimental replicates per group). **f** C57BL/6 mice were intravenously injected with the indicated formulations containing 40 μg SIINFEKL and 40 μg CpG on days 0 and 5, and the frequency of antigen-specific CD8α$^+$ T cells in peripheral blood was measured on day 10. Shown are the representative scatter plots (**g**) and frequency of antigen-specific CD8α$^+$ T cells on day 10 (**h**) ($n = 6$ mice for DOPE-LNV and $n = 5$ mice for all other groups). **i, j** The frequency of antigen-specific CD8α$^+$ T cells on day 10 in WT C57BL/6 and C3 KO C57BL/6 mice after vaccination as described above ($n = 5$ mice for WT and $n = 3$ mice for all other groups). Data were analyzed by one-way analysis of variance (ANOVA) with Tukey's multiple comparisons post-test. Data represent mean ± SEM. Figure 2f, created with BioRender.com, released under a Creative Commons Attribution-NonCommercial-NoDerivs 4.0 International license.

spleen (Supplementary Fig. 11b, c), further indicating spleen targeting is essential for nanovaccines to be fully functional.

To understand whether the phospholipid tail can affect the biodistribution and immune responses, we used DOPE, 1,2-dilauroyl-sn-glycero-3-phosphoethanol-amine (DLPE), 1,2-dimyristoyl-sn-glycero-3-phosphoethanolamine (DMPE), 1,2-dipalmitoyl-sn-glycero-3-phosphoethanolamine (DPPE), or 1,2-distearoyl-sn-glycero-3-phosphoethanolamine (DSPE), which have the same headgroup but different tails to prepare liposomes (Fig. 3a). It should be noted that the transition temperature (Tm) is increased in the order of DOPE, DLPE, DMPE, DPPE, and DSPE. We further quantified the liposomal membrane fluidity by using the Laurdan method and atomic force microscopy (AFM)[29–32] (Supplementary Fig. 12a–d), which was decreased in the order of DOPE, DLPE, DMPE, DPPE, and DSPE and well correlated with the Tm of these lipids. These liposomal formulations all exhibited similar sizes and zeta potentials (Supplementary Fig. 12e, f). Cryo-electron microscopy (cryo-EM) confirmed the homogeneous size distribution (Fig. 3b). Surprisingly, only DOPE had efficient accumulation in the spleen, while the spleen targeting efficiency of the other 4 phospholipids-based liposomes was much lower (Fig. 3c, d). Confocal microscopy of spleen sections indicated that DOPE liposomes accumulated in the spleen more efficiently than liposomes with other phospholipids (Fig. 3e). The most abundant protein bound to DLPE and DMPE-based liposomes was albumin, while the most abundant protein bound to DPPE and DSPE-based liposomes was the complement C3 (Fig. 3f). The different protein corona compositions can be ascribed to the apparent pKa values of these formulations (Supplementary Fig. 12g). Notably, although DOPE, DPPE, and DSPE could bind

https://doi.org/10.1038/s41467-024-52104-z

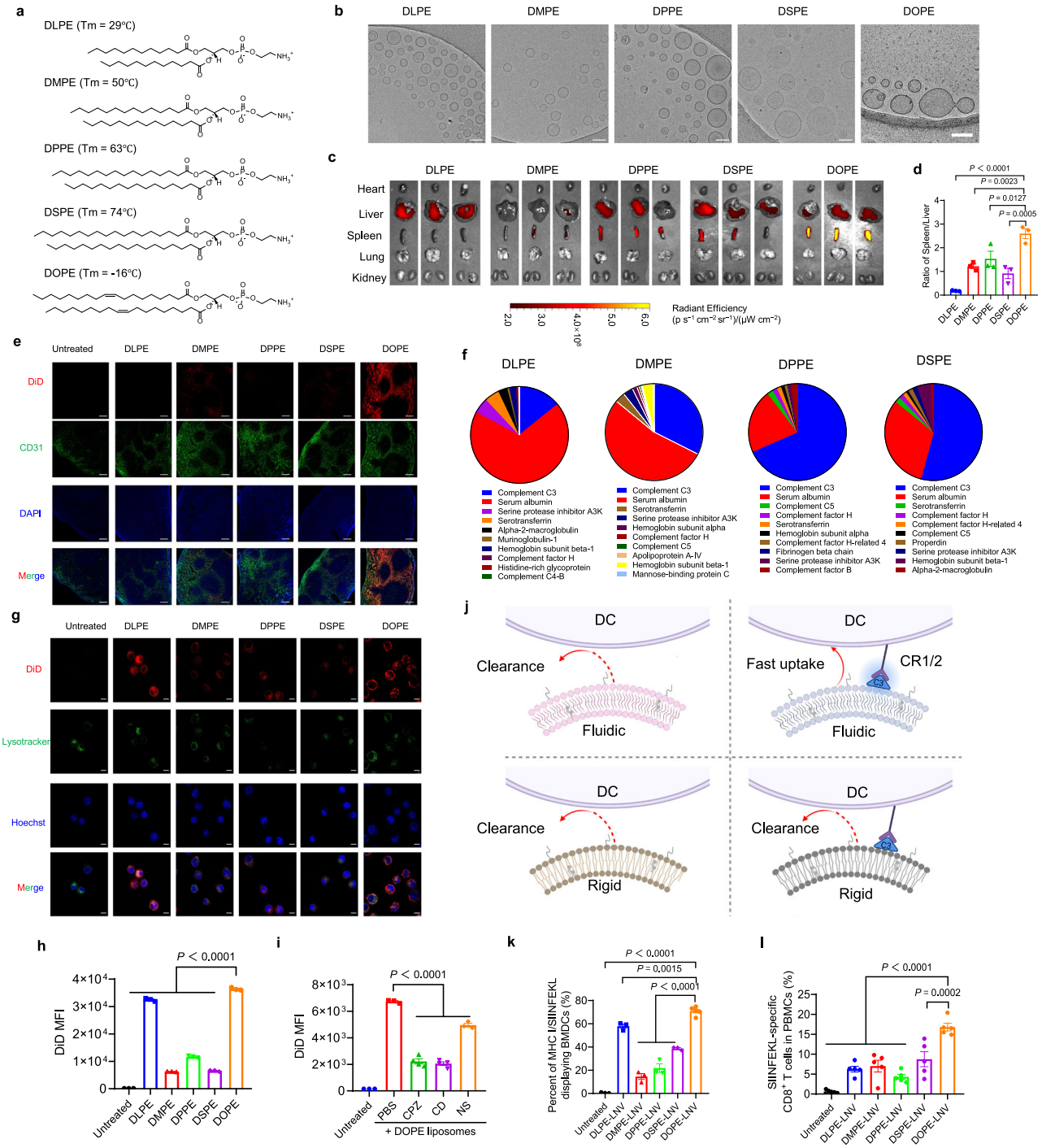

to the complement C3, DPPE, and DSPE failed to accumulate in the spleen, indicating factors other than the complement C3 also contributed to the spleen targeting. Interestingly, the cellular uptake efficiency was positively correlated with the fluidity of liposomes. In particular, the cellular uptake of fluidic DOPE liposomes by DC2.4 was much more efficient than rigid DPPE and DSPE liposomes (Fig. 3g, h). The efficient uptake of DOPE liposomes was mediated through multiple pathways, including clathrin-mediated endocytosis, macropinocytosis, and caveolin-mediated uptake, which was partially blocked by chlorpromazine (CPZ), cytochalasin D (CD), and nystatin (NS), respectively (Fig. 3i). We speculate that the C3-containing protein corona facilitated the initial arrest in the spleen and efficient cellular uptake by DC was required to achieve efficient retention in the spleen (Fig. 3j). In line with this, DOPE with both the complement C3 and high fluidity exhibited efficient spleen targeting. In contrast, DPPE and DSPE with the complement C3 but lacking high fluidity failed to accumulate in the spleen. Similarly, DLPE liposomes exhibiting efficient cellular uptake by DC but lacking the complement C3-containing corona failed to accumulate in the spleen, and DMPE liposomes lacking both efficient cellular uptake by DC and the complement C3 also failed to accumulate in the spleen (Fig. 3j). The complement C3 mainly utilizes the macropinocytosis pathway[33], so we focused more on whether this pathway plays a dominant role in vivo. We intravenously injected poly IC, a molecule that can selectively block macropinocytosis[18,34], into animals and then injected DOPE liposomes. As shown in Supplementary Fig. 13a, b, pretreating animals with poly IC significantly compromised the spleen targeting, as well as the cellular uptake of DOPE liposomes by multiple subsets of immune cells in the spleen, indicating

Fig. 3 | Fluidity and protein corona both affect the biodistribution and immune responses. a Chemical structures of phospholipids used for liposome preparation. **b** Cryo-electron microscopy (cryo-EM) of liposomes containing indicated phospholipids, scale bar = 100 nm. The data are representative of two independent experiments. **c** The biodistribution of indicated liposome formulations in C57BL/6 mice at 6 h post intravenous injection. **d** The ratio of indicated liposome formulations in the spleen and liver at 6 h post intravenous injection ($n = 3$ mice per group). **e** Immunofluorescence staining of spleen sections from animals receiving liposomes prepared with indicated lipids. The data are representative of two independent experiments, scale bar = 200 μm. **f** The composition of protein corona on liposomes prepared with indicated phospholipids. The data are representative of two independent experiments. Cellular uptake of liposomes containing indicated lipids by DC2.4. Shown are confocal images, scale bar = 10 μm (**g**) and quantification of the uptake by flow cytometry (**h**) ($n = 3$ experimental replicates per group). **i** Effect of different inhibitors on the cellular uptake of DOPE-liposomes by DC2.4 ($n = 3$ experimental replicates per group). **j** Schematic showing liposomes with the complement C3 and fluidic membrane can be efficiently taken up by spleen-resident dendritic cells, resulting in enhanced retention in the spleen. Liposomes lacking the complement C3 or lacking the fluidic membrane fail to be taken up by spleen-resident dendritic cells, resulting in poor retention in the spleen. **k** BMDCs were treated with indicated formulations for 6 h, and the antigen presentation was measured by flow cytometry. Shown are quantification of antigen presentation efficiency ($n = 3$ experimental replicates per group). **l** C57BL/6 mice were intravenously injected with the indicated formulations containing 40 μg SIINFEKL and 40 μg CpG on days 0 and 5, and the frequency of antigen-specific CD8α$^+$ T cells in peripheral blood was measured on day 10. Shown are the frequency of antigen-specific CD8α$^+$ T cells on day 10 ($n = 5$ mice per group). Data were analyzed by one-way analysis of variance (ANOVA) with Tukey's multiple comparisons post-test. Data represent mean ± SEM. Figure 3j, created with BioRender.com, released under a Creative Commons Attribution-NonCommercial-NoDerivs 4.0 International license.

that the macropinocytosis played an important role in vivo (Supplementary Fig. 13c, d). Consequently, LNV prepared with DLPE, DMPE, DPPE, DSPE, or DOPE had similar sizes and zeta potentials (Supplementary Fig. 14a, b), but DOPE-LNV induced much stronger antigen presentation than other phospholipids (Fig. 3k, Supplementary Fig. 14c). Notably, DOPE-LNV induced 2 to 4-fold stronger antigen-specific CD8α$^+$ T cells among PBMCs compared with other phospholipids (Fig. 3l, Supplementary Fig. 14d). Altogether, these results indicate that phospholipid's headgroup and tail can both affect the distribution and immune responses by tuning the protein corona and fluidity of nanovaccines.

Effect of ultrasound on intratumoral T cell infiltration

Having shown the excellent expansion of antigen-specific CD8α$^+$ T cells induced by DOPE-based LNV, we sought to recruit the expanded T cells to the tumor tissue. To achieve this, we loaded a hydrophobic sonosensitizer (IR780) to LNV to obtain LNVS. As the sonosensitizer and vaccine components can be efficiently loaded into liposomes within one step, this does not increase the complexity of manufacturing or quality control. LNVS exhibited good stability, and no significant change in particle size was observed before and after lyophilization (Supplementary Fig. 15a). Compared with DOPE-liposome carriers, DOPE-LNVS exhibited similar fluidity and complement C3-containing protein corona, indicating the low dose of antigen, CpG, and IR780 did not substantially influence the properties of DOPE-liposome carriers (Supplementary Fig. 15b–d). Notably, LNVS efficiently generated ROS in the presence of ultrasound (Supplementary Fig. 16a, b) and activated antigen-presenting cells (Supplementary Fig. 16c, d). In an in vitro Transwell system, treatment of tumor cells with LNVS + US followed by the addition of dendritic cells and T cells promoted T cell migration from the upper chamber to the bottom well, indicating LNVS + US had the potential to recruit T cells (Supplementary Fig. 17a, b). To learn the distribution kinetics of LNVS in the tumor, we intravenously injected DOPE-based LNVS or DOPE-based LNS (liposomal nano-sonosensitizer without antigen peptide and CpG) into MC38 tumor-bearing mice and imaged the fluorescence of IR780 in the tumor. Both DOPE-based LNVS and DOPE-based LNS passively accumulated in the MC38 tumor through the enhanced permeability and retention (EPR) effect, and the tumor accumulation reached a plateau between 8 and 24 h post-injection (Fig. 4a). All five phospholipids-based LNVS containing the same phospholipid tail accumulated in the tumor in a similar manner, indicating the EPR effect was not sensitive to the phospholipids used (Supplementary Fig. 18a, b). In the tumor tissue, DOPE-based LNVS was efficiently taken up by tumor cells and antigen-presenting cells (Supplementary Fig. 18c). DOPE-LNVS also exhibited accumulation in TC-1 and B16F10 tumors, indicating this approach may have broad applications (Supplementary Fig. 18d).

To learn whether ultrasound and sonosensitizer could recruit T cells in vivo, we intravenously injected LNV or LNVS into MC38 tumor-bearing mice on days 10 and 15. On days 11 and 16, ultrasound was applied to animals receiving LNVS (Fig. 4b). Compared with LNV, LNVS + US induced higher levels of chemokines (Fig. 4c) and higher levels of integrins and adhesion molecules such as ICAM-1 (intercellular adhesion molecule-1) and VCAM-1 (vascular cell adhesion molecule-1) on endothelial cells (CD31$^+$) in the tumor region (Supplementary Fig. 19a–c), which are beneficial for recruiting T cells[35,36]. Moreover, LNVS + US more efficiently induced activation of DCs in the tumor compared with other formulations (Fig. 4d–f). To further understand the impact of phospholipids and ultrasound treatment on programing T cell immunity, we harvested the tumor tissues on day 18 and analyzed the levels of T cells in the tumor using flow cytometry. DOPE-based LNV led to more antigen-specific CD8α$^+$ T cells in the tumor compared with other phospholipids-based LNV. This reflected the basal level of infiltration of T cells from the peripheral blood to the tumor. Strikingly, DOPE-based LNVS in combination with ultrasound led to 3-fold more infiltration of antigen-specific CD8α$^+$ T cells in the tumor compared with DOPE-based LNV ($P < 0.0001$) (Fig. 4g, h, Supplementary Fig. 20). These results indicate that while delivering LNVS to the tumor is important to create a microenvironment that can facilitate the recruitment of T cells, another more important aspect is to enhance the delivery to the spleen, which can significantly affect the overall expansion of antigen-specific T cells.

Therapeutic effect on MC38-OVA tumors

After confirming the excellent performance of DOPE-based LNVS + US on controlling the activation and intratumoral infiltration of antigen-specific CD8α$^+$ T cells, we aimed to investigate their therapeutic effect on tumor-bearing mice. To achieve this, we intravenously injected LNS, LNV, or LNVS into MC38-OVA tumor-bearing mice on days 10 and 15. Ultrasound was applied to the tumor region of animals receiving LNS or LNVS on days 11 and 16 (Fig. 5a). LNS + US (sonodynamic therapy) did not induce a detectable therapeutic effect. In contrast, LNV alone strongly inhibited the growth of tumors but failed to completely regress tumors. Remarkably, LNVS + US exhibited the most potent therapeutic effect and even regressed 2/6 tumor-bearing mice (Fig. 5b–d). Further analysis indicated that LNS + US did not induce any detectable level of antigen-specific CD8α$^+$ T cells among PBMCs, while LNV and LNVS + US both induced similar levels of antigen-specific CD8α$^+$ T cells among PBMCs (Fig. 5e, f). Importantly, LNV only slightly enhanced the intratumoral infiltration of antigen-specific CD8α$^+$ T cells, but LNVS + US significantly promoted the infiltration of antigen-specific CD8α$^+$ T cells compared with untreated control ($P < 0.0001$), LNS + US ($P < 0.001$), and LNV ($P < 0.001$) (Fig. 5g, h). These results indicate that the therapeutic effect was positively correlated with the levels of antigen-specific CD8α$^+$ T cells in the tumor

https://doi.org/10.1038/s41467-024-52104-z

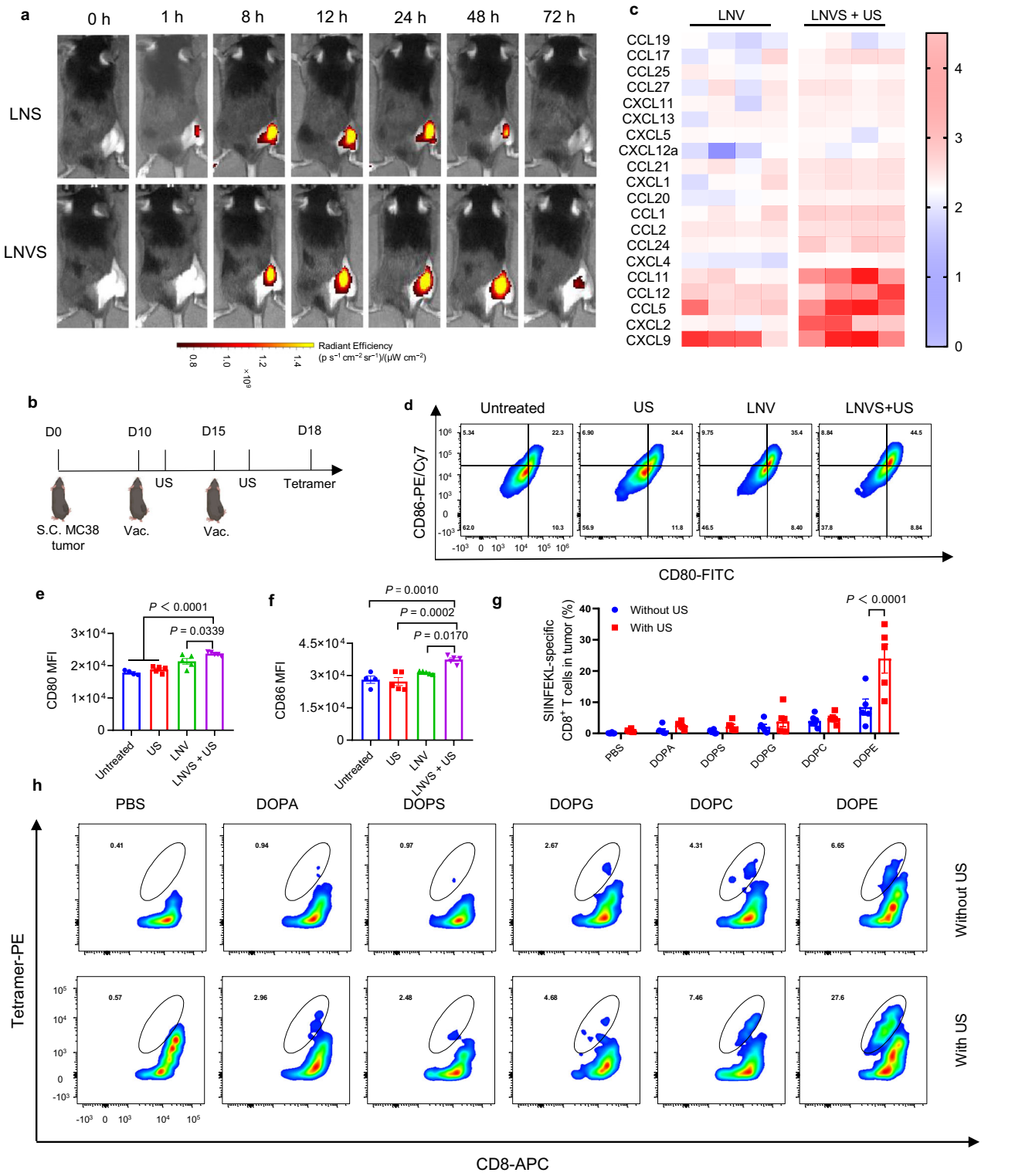

Fig. 4 | LNVS promotes the recruitment of antigen-specific T cells to the tumor in the presence of ultrasound. a The biodistribution of liposomal nano-sonosensitizer (LNS) and LNV containing sonosensitizer (LNVS) in the tumor at indicated time points ($n = 5$ mice per group). **b** C57BL/6 mice were inoculated subcutaneously with 1×10^6 MC38 tumor cells on day 0 and vaccinated with the indicated formulations on days 10 and 15. Ultrasound was applied to the tumor region on days 11 and 16. **c** Shown are the levels of chemokines in the tumor on day 18 ($n = 4$ mice per group). **d** Representative scatter plots for intratumoral DC activation and (**e**, **f**) expression levels of CD80 and CD86 on DC ($n = 4$ mice for WT and $n = 5$ mice for all other groups). **g**, **h** The frequency of antigen-specific CD8α⁺ T cells in the tumor on day 18 and representative scatter plots ($n = 5$ mice for DOPE and $n = 6$ mice for all other groups). Data were analyzed by one-way ANOVA (**e**, **f**) or two-way ANOVA (**g**) with Tukey's multiple comparisons post-test. Data represent mean ± SEM. Figure 4b, created with BioRender.com, released under a Creative Commons Attribution-NonCommercial-NoDerivs 4.0 International license.

https://doi.org/10.1038/s41467-024-52104-z

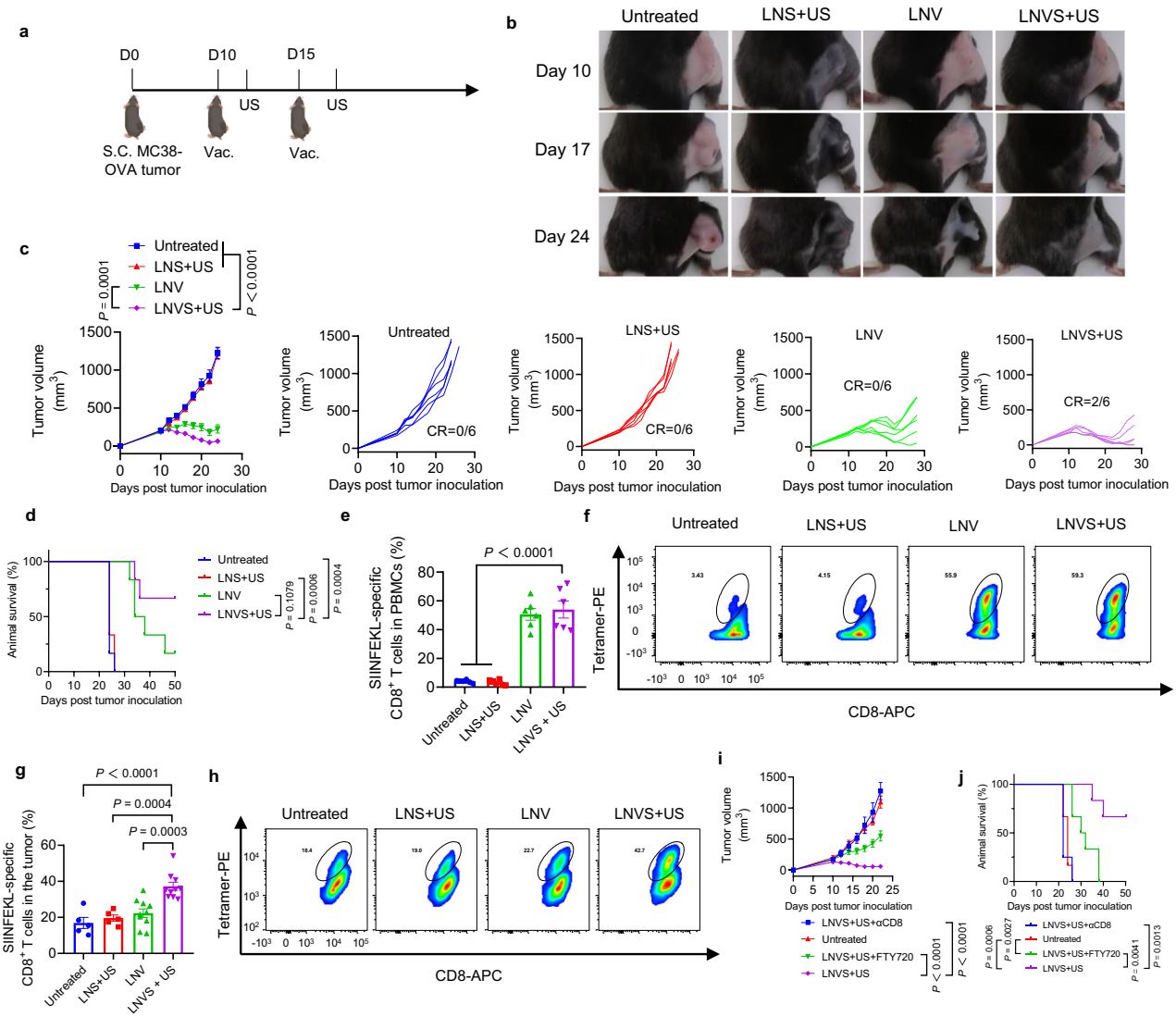

Fig. 5 | LNVS exhibits a potent therapeutic effect on MC38-OVA tumor-bearing mice. a C57BL/6 mice were inoculated subcutaneously with 1×10^6 MC38-OVA tumor cells on day 0 and vaccinated with the indicated formulations on days 10 and 15. Ultrasound was applied to the tumor region for selected groups on days 11 and 16. **b** Representative images of tumor-bearing mice treated with indicated formulations on different days. **c** Average and individual tumor growth curves for animals treated with indicated formulations ($n = 6$ mice per group) CR = complete regression. **d** The survival curves of animals treated with indicated formulations ($n = 6$ mice per group). Frequency of antigen-specific CD8α$^+$ T cells in PBMCs on day 18 (**e**) ($n = 6$ mice per group), and representative scatter plots (**f**). Frequency of antigen-specific CD8α$^+$ T cells in the tumor on day 18 (**g**) ($n = 5$ mice for Untreated and LNS + US, $n = 10$ mice for all other groups), and representative scatter plots (**h**). **i**, **j** Effect of FTY720 treatment and CD8α$^+$ T cell depletion on the therapeutic effect of LNVS + US ($n = 4$ mice for LNVS + US + αCD8 and $n = 6$ mice for all other groups). Data were analyzed by log-rank (Mantel–Cox) test (**d**, **j**), one-way ANOVA (**e**, **g**), or two-way ANOVA (**c**, **j**) with Tukey's multiple comparisons post-test. Data represent mean ± SEM. Figure 5a, created with BioRender.com, released under a Creative Commons Attribution-NonCommercial-NoDerivs 4.0 International license.

rather than in the peripheral blood. Notably, cDC1-deficient mice receiving LNVS + US exhibited weaker T cell responses and less tumor growth inhibition (Supplementary Fig. 21), indicating that cDC1 is particularly important for T cell priming and therapeutic efficacy. To further understand the role of infiltrating T cells, we took advantage of FTY720, which is known to deplete circulating T cells. Mice treated with FTY720 and LNVS + US had faster tumor growth and shorter survival compared with LNVS + US, indicating circulating T cells contribute to the therapeutic effect (Fig. 5i, j). Furthermore, the depletion of CD8α$^+$ T cells also compromised the therapeutic efficacy of LNVS + US ((Fig. 5i, j), further confirming the importance of CD8α$^+$ T cells. To learn whether animals "cured" by LNVS + US had acquired protective immunity, we rechallenged these "cured" animals with the same tumor cells on the contralateral side on day 60, and the age-matched mice were used as the control group. While the control group developed tumors and reached the endpoint within 26 days, the "cured" animals were free of tumors (Supplementary Fig. 22a–f). Moreover, we also observed the presence of effector memory T cells (CD44$^+$CD62L$^-$) and central memory T cells (CD44$^+$CD62L$^+$) in the peripheral blood of tumor-bearing mice (Supplementary Fig. 22g, h). Altogether, these results indicate that these animals have acquired immunity to protect them from relapse.

We performed additional experiments to demonstrate the abscopal effect. LNVS + US not only regressed the primary tumor (exposed to ultrasound) but also the distant tumor (not exposed to ultrasound), while other groups were less efficient at regressing primary and distant tumors compared with LNVS + US (Supplementary Fig. 23a–e).

https://doi.org/10.1038/s41467-024-52104-z

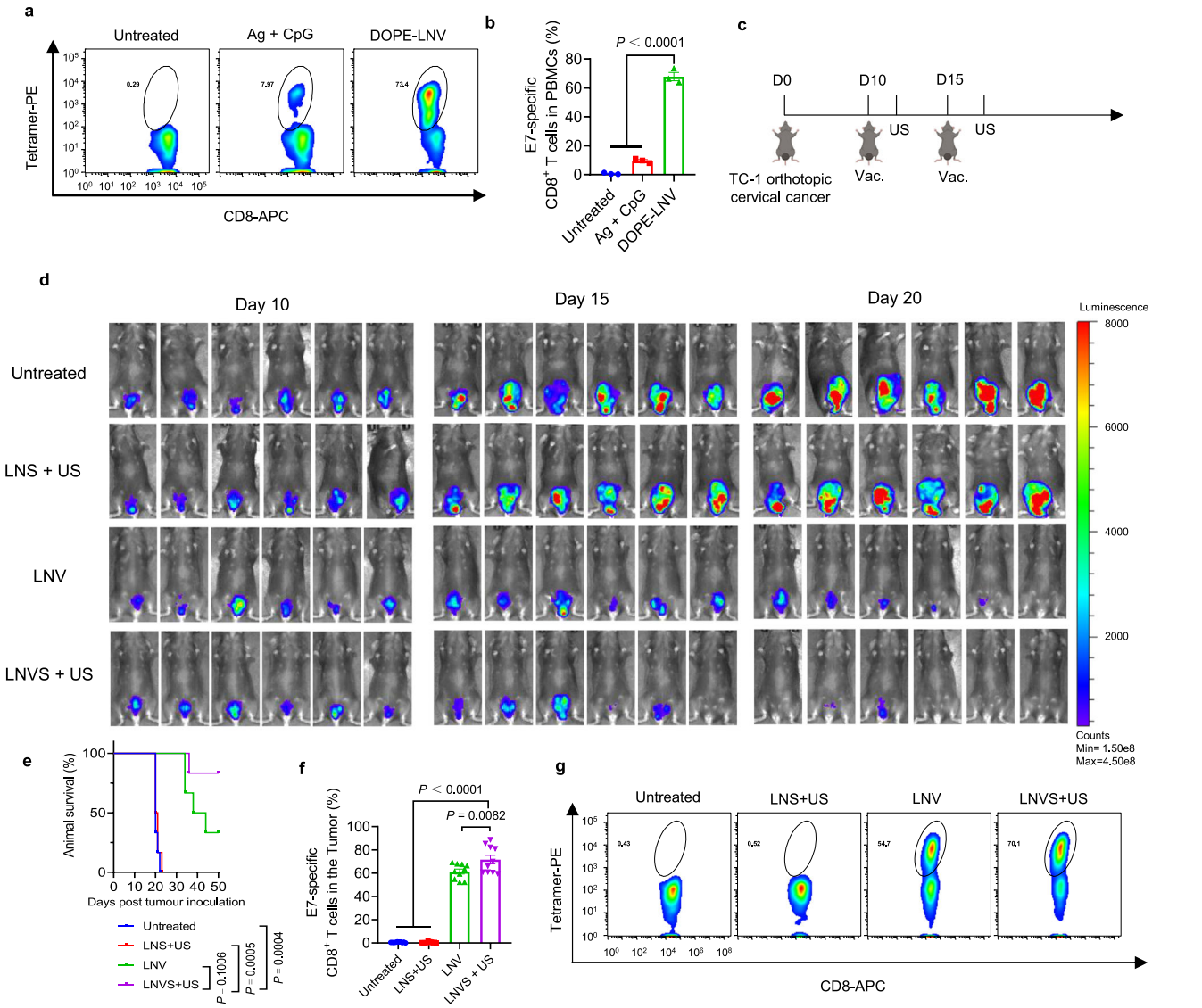

Fig. 6 | LNVS exhibits a potent therapeutic effect on orthotopic cervical cancer. Naïve C57BL/6 mice were intravenously vaccinated with indicated formulations on days 0 and 5, and the frequency of antigen-specific CD8α$^+$ T cells in peripheral blood was measured on day 10. Shown are the representative scatter plots (**a**) and frequency of antigen-specific CD8α$^+$ T cells on day 10 (**b**) ($n = 3$ mice per group). **c** C57BL/6 mice were inoculated with 1×10^6 TC1-luc cells in the vaginal tract on day 0. On days 10 and 15, animals were vaccinated with indicated formulations containing 20 μg E7 and 20 μg CpG. On days 11 and 16, ultrasound was applied to the tumor region of animals receiving LNS or LNVS (sonosensitizer dose is fixed at 40 μg/dose of IR780). Tumor burden was monitored over time using an IVIS imaging system (**d**) ($n = 6$ mice per group). **e** Survival of orthotopic cervical cancer-bearing mice after treatment with indicated formulations ($n = 6$ mice per group). Frequency of antigen-specific CD8α$^+$ T cells in the tumor on day 20 (**f**) ($n = 10$ mice per group), and representative scatter plots (**g**). Data were analyzed by one-way analysis of variance (ANOVA) with Tukey's multiple comparisons post-test (**b**, **f**) or log-rank (Mantel–Cox) test (**e**). Data represent mean ± SEM. Figure 6c, created with BioRender.com, released under a Creative Commons Attribution-NonCommercial-NoDerivs 4.0 International license.

Therapeutic effect on orthotopic tumors

To pressure test the performance of LNVS + US, we aimed to use a more challenging tumor model, the orthotopic cervical cancer, which has low levels of antigen-specific CD8α$^+$ T cells[37]. We first tested whether DOPE-based LNV could induce a potent T cell response against the E7 antigen expressed by TC1 tumor cells. Two doses of DOPE-based LNV induced ~70% E7-specific CD8α$^+$ T cells among PBMCs, which were about 10-fold stronger than that of the soluble vaccine (Fig. 6a, b). The frequency of E7-specific CD8α$^+$ T cells was above 60% when DOPE-LNV had 5–40 μg of antigens and CpG. Reducing the dose to 2.5 μg or 1 μg significantly compromised the antigen-specific T cell responses (Supplementary Fig. 24). LNV and LNVS both induced similar levels of E7-specific CD8α$^+$ T cells (Supplementary Fig. 25), indicating the sonosensitizer did not interfere with the activation of T cells.

We next evaluated the therapeutic effect on orthotopic cervical cancer. To achieve this, we intravenously injected LNS, LNV, or LNVS into orthotopic TC1 tumor-bearing mice on days 10 and 15. Ultrasound was applied to the tumor region of animals receiving LNS or LNVS (Fig. 6c) on days 11 and 16. LNS + US did not induce a significant therapeutic effect. LNV exhibited strong tumor suppression effect, but only 2/6 animals had complete regression. Remarkably, LNVS + US exhibited the most potent therapeutic effect, and 4/6 animals had complete regression (Fig. 6d). Accordingly, animals treated with LNVS + US had longer survival than LNV or LNS + US (Fig. 6e). Further analysis indicated that the untreated group and LNS + US group did not have any detectable level of antigen-specific CD8α$^+$ T cells in the tumor. LNV increased intratumoral antigen-specific CD8α$^+$ T cells as T cells expanded in the spleen could migrate to the tumor. LNVS + US

increased the level of intratumoral antigen-specific CD8α⁺ T cells compared with LNV ($P < 0.01$) and induced 147-fold more antigen-specific CD8α⁺ T cells than traditional sonodynamic therapy LNS + US ($P < 0.0001$), thus further enhancing the therapeutic effect (Fig. 6f, g). Animals "cured" by LNVS + US were protected from lung metastasis, while age-matched control mice exhibited severe metastasis and reached the endpoint within 42 days (Supplementary Fig. 26a–c). Moreover, we also observed the presence of effector memory T cells ($CD44^+CD62L^-$) and central memory T cells ($CD44^+CD62L^+$) in the peripheral blood of orthotopic TC1 tumor-bearing mice (Supplementary Fig. 26d, e). These results indicate that these animals have acquired immunity to prevent relapse. We next used LNVS + US to treat animals with established orthotopic cervical cancer and lung metastasis. Under this condition, LNVS + US not only regressed the orthotopic cervical cancer (exposed to ultrasound), but also regressed the lung metastasis (not exposed to ultrasound) (Supplementary Fig. 27a–c). Notably, all formulations were well tolerated, and no body weight decrease was observed throughout the therapeutic study (Supplementary Fig. 28). Moreover, the histological analysis indicated no changes to major organs were observed (Supplementary Fig. 29), further confirming the excellent safety profiles of these formulations.

Finally, we assessed the immune responses against Trp1 expressed on melanoma. Two doses of LNV induced ~48.86% Trp1-specific IFN-γ⁺CD8α⁺ T cells among PBMCs, which were about 92 folds stronger than the soluble vaccine (Supplementary Fig. 30a, b). The frequency of Trp1-specific IFN-γ⁺CD8α⁺ T cells increased from 24.1 to 48.86% over the dose of 10–30 μg, followed by a decrease at the dose of 40 μg. Animals treated with LNVS + US exhibited slower tumor growth and longer survival than LNV or LNS + US (Supplementary Fig. 30c–j). LNV and LNVS + US exhibited similar levels of antigen-specific T cells in peripheral blood, but LNVS + US increased the level of intratumoral antigen-specific CD8α⁺ T cells compared with LNV ($P < 0.01$) and induced 4-fold more antigen-specific CD8α⁺ T cells than traditional sonodynamic therapy LNS + US ($P < 0.0001$). Altogether, our LNVS + US represents a promising strategy to program T cell immunity against different antigens and may have broad applications in the future.

Discussion

In this study, we tune the fluidity and protein corona of ultrasound-responsive liposomal naovaccines (LNVS) to program T cell immunity. Coupled with the targeted use of ultrasound over the tumor region, we can precisely recruit T cells to where they are needed, resulting in 60–80% antigen-specific intratumoral T cells. As far as we know, this is the highest level of antigen-specific T cells in the tumor achieved so far by using nanoparticle-based vaccines. LNVS + US exhibit potent therapeutic effects on MC38 tumors and orthotopic cervical cancer and protect cured animals from relapse. Moreover, no severe side effects are observed throughout the entire study, indicating the excellent safety profile of our strategy.

Efficient accumulation in the spleen is critical for maximal expansion of antigen-specific CD8α⁺ T cells[16,17]. Although previous studies have reported the effect of nanoparticles' surface properties (e.g., the negatively charged phospholipid DOPA and the resulting β2-glycoprotein 1-containing protein corona) on spleen targeting, how the fluidity and protein corona work together to regulate the spleen targeting and T cell responses of liposomes remains unclear. Understanding the impact of fluidity/protein corona on spleen targeting can provide new insights to precisely control how nanoparticles interact with target cells and design effective formulations for vaccine delivery. Among all the lipids tested, we found that the neutral phospholipid DOPE-based liposomes had the best spleen targeting efficiency. Indeed, the potential of DOPE for spleen targeting has been noted before[38], but the underlying regulation mechanism and the impact on T cell immunity have not been explored. This motivated us to investigate the underlying mechanism and explore its potential for programing T cell immunity. We first prepared a small library of liposomes with different protein corona compositions and fluidities. In particular, the most abundant protein bound to DOPA-based liposomes was β2-glycoprotein 1, which was consistent with previous reports involving the use of DOPA-based LNP for spleen targeting[19,20], while the most abundant protein bound to DOPS, DOPG, and DOPC-based liposomes was albumin. Notably, DOPE-based liposomes had the most complement C3 bound to the surface, indicating that the complement C3 might be critical for the spleen targeting of DOPE-based liposomes[33,39–41]. Indeed, knocking out complement C3 compromised the spleen targeting of DOPE-based liposomes, further confirming the critical role of complement C3 in mediating the accumulation of liposome carriers in the spleen. Interestingly, replacing the tail of DOPE with other saturated carbon chains (low fluidity or high stiffness) also compromised the spleen targeting and T cell immunity, although the protein corona might be similar to that of DOPE-liposomes. These results indicate that the protein corona is not the only factor affecting the interaction between liposomes and the body. Further analysis indicated that for the same phospholipid headgroup, the lipid tail with a higher fluidity exhibited more efficient cellular uptake by dendritic cells. This phenomenon is consistent with previous studies showing cells exhibit greater uptake of soft nanoparticles compared with hard nanoparticles[42]. Altogether, our results, therefore, indicate that the spleen targeting was dependent on the C3-containing protein corona and fluidity of liposomes because knocking out C3 or decreasing the fluidity (increasing the stiffness) of liposomes compromised the spleen targeting. The liposome size or morphology may impact APC uptake and DC activation, but all formulations share similar sizes and shapes in our study, so the effect of these factors is canceled. Moreover, although it is technically challenging to compare mRNA and peptide vaccines, as the optimal dose, composition, and dosing regimen can differ, peptide vaccines generally have better stability and do not require in vivo expression. Coupled with the strong immune responses and therapeutic effect of LNV-based peptide vaccine, we believe this platform may complement the use of mRNA vaccines in the clinic.

Recruiting antigen-specific CD8α⁺ T cells to the tumor tissue is another critical step for effective cancer immunotherapy. As DOPE-LNV with the C3-containing protein corona and high fluidity (low stiffness) exhibited more efficient spleen targeting and T cell activation than other phospholipids-based LNV, we focused on this formulation (which was further loaded with a sonosensitizer to obtain LNVS) for therapy. In the proof-of-concept study, we did not use additional strategies to tune the tumor accumulation of LNVS, as LNVS exhibited some passive accumulation in the tumor, which was sufficient to respond to ultrasound to upregulate chemokines and adhesion molecules[35,36], and facilitate the T cell infiltration in the tumor. Future studies are warranted to precisely control the specific targeting of LNVS in the spleen or tumor in a broader range. Moreover, although sonodynamic therapy (SDT) is emerging as a safe and noninvasive strategy for cancer therapy, the SDT's overall efficacy remains limited. In the proof-of-concept study, ultrasound serves as a safe and noninvasive tool to "pull" T cells "expanded" by the identified LNVS with the C3-containing protein corona and high fluidity (low stiffness), which has not been reported. From the perspective of clinical translation, our platform is also compatible with other approaches, such as high-intensity focused ultrasound (HIFU) or irradiation, which can directly establish a suitable tumor microenvironment for T cell infiltration without requiring intratumoral nanovaccines[43–48]. Moreover, depleting circulating T cells with FTY720 significantly compromised the therapeutic effect of LNVS + US, further confirming the importance of recruiting circulating T cells to the tumor is critical[1,12]. Notably, DOPE-based LNVS + US led to more T cells in the tumor compared with other phospholipids-based LNVS + US. These results indicate that while delivering LNVS to the tumor is important to create a

microenvironment that can facilitate the recruitment of T cells, another more important aspect is to tune the biodistribution outside the tumor, especially to enhance the delivery to the spleen, which can significantly affect the overall expansion of antigen-specific T cells.

In summary, we have developed a designer ultrasound-responsive nanovaccine LNVS to program T cell immunity by targeting the spleen and tumor. The headgroup and tail of phospholipid are both critical for determining the spleen targeting by tuning the protein corona and fluidity of liposomes, which further affect the T cell responses. Moreover, LNVS utilizes the EPR effect to accumulate in the tumor, where it responds to external ultrasound to promote infiltration of antigen-specific $CD8\alpha^+$ T cells, resulting in potent antitumor effects. Depleting circulating T cells or depleting total $CD8\alpha^+$ T cells significantly compromises the therapeutic effect, indicating peripheral T cells contribute to the therapeutic effect. As LNVS only requires one neutral phospholipid DOPE, it may simplify the manufacturing process and facilitate the clinical translation for cancer immunotherapy.

Methods

Ethics statement

This research complies with all relevant ethical regulations. All work performed on animals was in accordance with and approved by the University Committee on Use and Care of Animals at Tsinghua University. Animals were housed in 12 h light/12 h dark cycles, 65–75 °F (~18–23 °C), and 40–60% humidity. Animals were euthanized by CO_2 inhalation, followed by cervical dislocation when the tumor reached 15 mm in any dimension or when they became moribund with severe weight loss or unhealing ulceration. This limit was not exceeded at any point.

Synthesis of phospholipid-modified antigen peptides

Phospholipid-modified antigen peptides were synthesized as reported previously[7]. Briefly, CSSSIINFEKL, CRAHYNIVTF, or CTAPDNLGYM (Genscript) was reacted with Dioleoyl-sn-glycero-3-phosphoethanolamine-N-[3-(2-pyridyldithio) propionate] (Sigma) at a 1.5:1 molar ratio in DMF for 3 h at room temperature. The obtained phospholipid-antigen was diluted 10X with DI water and freeze-dried before preparing liposomal nanovaccines.

Preparation and characterization of liposomal nanovaccines (LNV)

For the preparation of liposomal nanovaccines (LNV), 1,2-dioleoyl-sn-glycero-3-phosphoethanolamine (DOPE), cholesterol, DOPE-PEG_{5000}, and phospholipid-modified antigen peptides (molar ratios = 65:32.5:2.5:1.6) were dissolved in ethanol, which was mixed with DI water containing cholesterol-CpG (General Biol) at a volume ratio of 1:10 and then homogenized using an extruder equipped with a 400-nm polycarbonate membrane. For the preparation of LNV with phospholipids containing different headgroups or tails, other phospholipids such as 1,2-dioleoyl-sn-glycero-3-phosphate (sodium salt) (DOPA), 1,2-dioleoyl-sn-glycero-3-phospho-L-serine (sodium salt) (DOPS), 1,2-dioleoyl-sn-glycero-3-phospho-(1'-rac-glycerol) (sodium salt) (DOPG), 1,2-dioleoyl-sn-glycero-3-phosphocholine (DOPC), 1,2-dilauroyl-sn-glycero-3-phosphoethanol-amine (DLPE), 1,2-dimyristoyl-sn-glycero-3-phosphoethanolamine (DMPE), 1,2-dipalmitoyl-sn-glycero-3-phosphoethanolamine (DPPE), and 1,2-distearoyl-sn-glycero-3-phosphoethanolamine (DSPE) were used to replace DOPE and the same protocol described above was used to prepare LNV. Liposome carriers were prepared using the same protocol without adding antigen peptide antigens and CpG. For biodistribution studies, DiR was mixed with lipids in the ethanol solution, followed by homogenization described above to obtain DiR-labeled liposome carriers or DiR-labeled LNV that contain a final concentration of 0.625 μg/ml DiR. LNVS was prepared similarly except that the sonosensitizer IR780 was added to the ethanol phase when preparing LNV. The size and zeta potential were measured by dynamic laser scattering (DLS) on a Malvern Zetasizer. The antigen peptide and CpG concentrations were analyzed by LavaPep (Gel company) or gel electrophoresis following previously reported protocols[49,50]. The concentration of sonosensitizer was quantified by measuring the fluorescence of IR780. For cryo-EM, 4 μl of sample (6 mg/ml) was dropped on a glow discharged copper grid coated with holey carbon (R 2/2; Quantifoil, Jena, Germany), and plunge-freezing was performed through Vitrobot Mark IV cryo plunger (ThermoFisher Scientific, Hillsboro, OR), with a wait time of 2 min and a blot time of 3.5 or 4.0 s. The samples were loaded on a 200 kV FEI Talos Arctica transmission electron microscope (ThermoFisher Scientific, Hillsboro, OR) equipped with a K2 direct electron detector (Gatan, CA). Images were recorded in counting mode at nominal magnifications of 17500 × or 28,000 × (pixel size, 2.41 Å or 1.51 Å) and at a defocus of −3.0 μm in SerialEM[51]. For each image, a movie consisting of 32 frames was recorded by a total dose of 40 $e^-/Å^2$ or 50 $e^-/Å^2$. The frames of each movie were corrected for the electron-beam induced motion and averaged into a micrograph using MotionCor2[52].

ROS generation, BMDC activation, and T cell migration in vitro

Throughout the studies, all cells were tested negative for mycoplasma contamination and morphologically confirmed. To quantify ROS generation, MC38 cells were treated with indicated formulations containing 1 μg/ml antigen, 1 μg/ml CpG, or 2 μg/ml sonosensitizer for 24 h. Then the old medium was replaced with fresh medium containing 2′,7′-Dichlorodihydrofluorescein diacetate (DCFH-DA, 1:2000 dilution), which became fluorescent upon ROS generation. Ultrasound (US) (2 W/cm^2, 50% duty cycle, 1 MHz, 5 min) was applied to indicated groups. The contact between each tissue culture well bottom and the ultrasound-emitting probe was facilitated using an ultrasound gel (Dandelion). After incubation for 20 min at 37 °C, the fluorescence was measured on a microplate reader (BioTek). To measure the activation of BMDCs (bone marrow-derived dendritic cells), MC38 cells were treated with indicated formulations in the absence or presence of ultrasound (2 W/cm^2, 50% duty cycle, 1 MHz, 5 min). After 24 h, BMDCs were added and incubated for another 24 h before measuring CD80/86 on BMDCs using flow cytometry. To monitor the effect of LNVS + US on T cell migration in vitro, 2×10^5 MC38-OVA cells were treated with indicated formulations containing 1 μg/ml antigen, 1 μg/ml CpG, or 2 μg/ml sonosensitizer) for 24 h. Then ultrasound (US) (2 W/cm^2, 50% duty cycle, 1 MHz, 5 min) was applied to indicated groups. After 24 h, 2×10^5 BMDCs were added and incubated for another 24 h, and then 3.75×10^5 T cells were added to the upper chamber. After 3 h, the percentages of T cells in the bottom well were measured by flow cytometry.

Pharmacokinetics and biodistribution

For the pharmacokinetic study, female C57BL/6 mice of age 6–8 weeks (Vital river) were intravenously injected with indicated formulations containing 5 μg/ml DiR. At predetermined time points, the blood samples were collected by retro-orbital bleeding. The fluorescence of DiR was observed by using the IVIS optical imaging system. For the biodistribution study on naïve mice, female C57BL/6 mice of age 6–8 weeks (Vital river) were intravenously injected with indicated formulations containing 0.625 μg/ml of DiR. After 6 h, animals were euthanized, and major organs such as the heart, liver, spleen, lung, and kidneys were harvested and imaged using an IVIS optical imaging system. In some experiments, a series of spleen sections from animals receiving indicated formulations were prepared and stained with anti-CD31 (clone: EPR172597) and DAPI. The slides were then observed by a confocal microscope (Zeiss LSM880). To analyze the uptake of liposomes by different subsets of cells, the spleens were prepared into single-cell suspension. The cells were incubated with CD16/32 for 10 min and then incubated with anti-F4/80 (clone: BM8), anti-CD11c (clone: N418), anti-CD3 (clone: 17A2), anti-CD45R/B220 (clone: RA3-

6B2), and anti-NK-1.1 (clone: PK136) on ice for 20 min before flow cytometry (BD LSRFortessa SORP) to analyze the uptake of liposomes by different subsets of immune cells in the spleen. In some experiments, C3 KO female C57BL/6 mice (Shanghai Model Organisms Center, Inc.) were intravenously injected with DOPE-based liposomes, and the biodistribution study was performed by following the above protocol.

Analysis of protein corona

The protein corona on liposomes containing different phospholipids was analyzed using a previously reported protocol[20,53]. Briefly, liposomes were prepared as described above and diluted with PBS (1X) to a final lipid concentration of 1 mg/ml. Mouse plasma was added to each liposome formulation at a 1:1 volume ratio and incubated at 37 °C for 15 min. The obtained mixture was loaded onto a 0.7-M sucrose with an equal volume to the mixture and centrifuged at 15,300 g and 4 °C for 1 h. The supernatant was carefully removed, and the pellet was washed with PBS (1X) and centrifuged at 15,300 g and 4 °C for 5 min. The washing was performed for a total of 2 times to obtain the complex of plasma proteins bound to nanoparticles, which were submitted to Bio-Tech Pack for mass spectrometry analysis.

Measurement of liposome fluidity and stiffness

The liposomal membrane fluidity was measured by using an in-house Laurdan probe sensitive to the membrane polarity[29–32]. Briefly, 3 mg/ml liposomes were incubated with an 8 mM Laurdan probe in a water bath at 60 °C. Then the fluorescence emission spectrum was recorded from 380 to 600 nm on a microplate reader (BioTek) at 45 °C. The generalized polarization (GP) parameter was calculated using the following equation: $GP = (I_{350}\text{-}I_{450})/(I_{350} + I_{450})$, where I_{350} is the fluorescence emission intensity at 350 nm (gel phase), and I_{450} is the fluorescence emission intensity at 450 nm (liquid crystalline phase). The stiffness of liposomes was measured by atomic force microscopy (AFM) at Shiyanjia Lab (www.shiyanjia.com) following the previously reported method with slight modifications. Briefly, liposomes in ddH_2O (20 µl) were incubated on the mica surface and air-dried. AFM force measurements were performed on a Bruker Dimension Icon AFM with RTESPA-150 tips. The AFM was performed in the peak force QNM mode.

Analysis of apparent pKa

The apparent pKa was measured following previous studies with slight modifications[20,54]. Briefly, liposome formulations (60 µM total lipids) and the TNS probe (2 µM) were incubated with a series of buffers containing 20 mM sodium phosphate, 25 mM citrate, 20 mM ammonium acetate, and 150 mM NaCl (the pH ranged from 2.5 to 12.5). The fluorescence intensity was measured using a microplate reader (Bio-Tek) at Ex = 325 nm and Em = 435 nm. Data were normalized to pH 2.5 and the apparent pKa is defined by the pH at half-maximum fluorescence.

Cellular uptake by dendritic cells

To image the cellular uptake of liposomes by dendritic cells, 2.5×10^5 DC2.4 cells were incubated with indicated formulations containing 0.25 µg/ml DiD for 6 h. Then the cells were washed with PBS and stained with Hoechst before observation by a confocal microscope (Zeiss LSM780). To quantitatively measure the cellular uptake of liposomes, 2.5×10^5 DC2.4 cells were incubated with indicated formulations containing 0.25 µg/ml DiD for 6 h. The cells were harvested and washed twice with FACS buffer before flow cytometry (BD LSRFortessa SORP). In some experiments, uptake inhibitors CPZ (10 µg/ml), CD (2.5 µg/ml), and NS (10 µg/ml) were added to cells. The cellular uptake was measured by flow cytometry, as described above.

Antigen uptake and immune cell activation in vivo

To learn the uptake of antigens and liposome carriers in vivo, female C57BL/6 mice of age 6–8 weeks (Vital river) were intravenously injected with DOPE-based liposomes containing 0.3 µg/ml of DiR and 200 µg/ml of FITC-antigen. After 6 h, animals were euthanized, and spleens were prepared into single-cell suspension to analyze the uptake of FITC-antigen and DiR by different subsets of cells. To learn the immune cell activation and cytokine secretion, mice were intravenously injected with DOPE-LNV (20 µg antigen and 20 µg CpG). After 24 h, peripheral blood and spleen were collected to measure the mean fluorescence intensity of CD69 expression on $CD8^+$ T cells. Serum was collected at predetermined time points, and production of IFN-β was determined using the ELISA kit (LumiKine™ Xpress mIFN-β 2.0, InvivoGen) following the manufacturer's instructions.

Vaccination studies

For vaccination studies on naïve mice, female C57BL/6 mice of age 6–8 weeks (Vital river) were intravenously injected with different formulations containing antigen peptides (40 µg) and CpG (40 µg) in 200 µl 10% sucrose on days 0 and 5. On day 10, the peripheral blood was collected through submandibular bleeding to analyze the frequency of antigen-specific $CD8\alpha^+$ T cells. For the dose dependence study, different doses of antigens (1–40 µg) and CpG (1–40 µg) were used.

For vaccination studies on tumor-bearing mice, female C57BL/6 mice of age 6–8 weeks (Vital river) were subcutaneously inoculated with 1×10^6 MC38 cells on day 0. On days 10 and 15, tumor-bearing mice were intravenously injected with different formulations containing antigen peptides (20 µg) and CpG (20 µg) in 200 µl 10% sucrose. On days 11 and 16, mice were anesthetized with isoflurane, and the tumors were treated with ultrasound (1 MHz, 2 W/cm^2, 50% duty cycle, 5 min), and contact between the emitting surface of the ultrasound transducer and the tumor surface was facilitated using an ultrasound gel (Dandelion)[55]. On day 18, animals were euthanized, and tumors were harvested to analyze the frequency of antigen-specific T cells. In some experiments, the tumor tissues harvested on day 18 from selected groups were submitted to RayBiotech, Inc.,Guangzhou, for analysis of chemokines. To learn the role of the spleen, female C57BL/6 mice were subjected to splenectomy one week before intravenous injection of DOPE-LNV on days 0 and 5. On day 10, the peripheral blood and lymph nodes were collected to analyze the frequency of antigen-specific $CD8\alpha^+$ T cells as described above.

Analysis of T cell responses

The frequency of antigen-specific $CD8\alpha^+$ T cells among PBMCs was analyzed by the tetramer staining as described previously[7]. Briefly, 150 µl of blood was collected from indicated groups, and red blood cells were lysed using Ammonium-Chloride-Potassium (ACK) lysis buffer. PBMCs were then washed with FACS buffer and blocked with anti-CD16/32 antibody for 10 min. Then cells were incubated with peptide-MHC tetramer (H-$2K^b$-restricted SIINFEKL or H-$2D^b$-RAHYNIVTF) for 30 min at room temperature and stained with anti-CD8α (53-6.7) on ice for 20 min. Cells were washed twice with FACS buffer and resuspended in DAPI before flow cytometry.

For intracellular cytokine staining (ICS) assay[56], 150 µl peripheral blood collected from vaccinated mice was lysed with ACK lysis buffer, washed with PBS, and plated at 10 million cells per ml in 50 µl T cell media (RPMI 1640 supplemented with 10% FBS, 2 mM glutamine, 55 µM β-mercaptoethanol, 1 mM pyruvate, 1% PS, 100 µg /ml HEPES, and non-essential amino acids) in 96-well U bottom plates. Cells were pulsed with 30 µg/ml antigen peptides (SIINFEKL or CTAPDNLGYM) for 6 h, with brefeldin A added during the last 4 h of incubation. Cells were then washed twice with ice-cold FACS buffer, followed by incubation with anti-CD16/32 for 10 min and anti-$CD8\alpha^+$ for 20 min on ice.

Cells were then fixed and permeabilized for 20 min on ice and then stained with anti-IFN-γ for 30 min on ice. After extensive washing, cells were analyzed by flow cytometry.

The frequency of antigen-specific CD8α$^+$ T cells in the tumor was analyzed following previously reported protocols[57,58]. Briefly, tumor tissues were cut into small pieces (2–4 mm), and cells were immersed in a digestion buffer containing collagenase type IV (1 mg/ml) and deoxyribonuclease I (100 μg/ml) in serum-free RPMI for 20 min at 37 °C under gentle shaking. The obtained mixture was further passed through a 70-μm strainer to obtain single-cell suspension. Then cells were incubated with peptide-MHC tetramer (H-2K^b-restricted SIINFEKL or H-2D^b-RAHYNIVTF) for 30 min at room temperature and stained with anti-CD45 (30-F11), anti-CD3 (17A2) and anti-CD8α (53-6.7) on ice for 20 min. Cells were washed twice with FACS buffer and resuspended in DAPI before flow cytometry.

Adhesion molecule detection

To measure adhesion molecules and integrins on the vasculature of the tumor region, female C57BL/6 mice of age 6–8 weeks (Vital river) were inoculated with 1×10^6 MC38 tumor cells on the right flank through subcutaneous injection on day 0. On days 10 and 15, tumor-bearing mice were intravenously injected with different formulations containing antigen peptides (20 μg), CpG (20 μg), and sonosensitizer (40 μg IR780) in 200 μl 10% sucrose. On days 11 and 16, ultrasound (1 MHz, 2 W/cm^2, 50% duty cycle, 5 min) was applied to the tumor region for selected groups. On day 18, animals were euthanized and tumors were harvested and prepared into single-cell suspensions as described above, followed by staining with anti-CD31 (clone: 390), anti-ICAM-1 (clone: YN1/1.7.4), anti-VCAM-1 (clone: 429 (MVCAM.A)) and anti-integrin-β1 (clone: HMβ1-1) before flow cytometry.

Therapeutic studies on MC38-OVA tumors

For therapeutic studies on MC38-OVA tumor-bearing mice, female C57BL/6 mice of age 6–8 weeks (Vital river) were inoculated with 1×10^6 MC38-OVA tumor cells on the right flank through subcutaneous injection on day 0. On days 10 and 15, tumor-bearing mice were intravenously injected with different formulations containing antigen peptides (20 μg), CpG (20 μg), and sonosensitizer (40 μg IR780) in 200 μl 10% sucrose. On days 11 and 16, ultrasound (1 MHz, 2 W/cm^2, 50% duty cycle, 5 min) was applied to the tumor region for selected groups. Tumor growth was monitored every 2 days, and the tumor volume was calculated using the following equation: tumor volume = length × width^2 × 0.52. Animals were euthanized when individual tumor sizes reached 15 mm in any dimensions or when animals exhibited severe weight loss or active ulceration. To learn the effect of circulating T cells, 1.25 mg/kg FTY720 was i.p. injected daily for the duration of the therapeutic study once LNVS was injected[59]. To deplete CD8$^+$ T cells, 200 μg/dose anti-mouse CD8α (Bio X Cell) was i.p. injected on days −2, 0, 2, 6, 13 and 20 of sample injection[60]. In some experiments, cured animals were rechallenged with 1×10^6 MC38-OVA cells on the left flank on day 60, and age-matched naïve mice were used as the control group and inoculated with 1×10^6 MC38-OVA tumor cells on the left flank. Tumor growth was monitored as described above.

Therapeutic studies on orthotopic cervical cancer

To establish the orthotopic cervical cancer model, female C57BL/6 mice were s.c. injected with medroxyprogesterone (3 mg/mouse) for diestrus synchronization on day −3. On day 0, the animals were inoculated with 1×10^6 TC1-luc cells by intravaginal administration. On days 10 and 15, tumor-bearing mice were intravenously injected with indicated formulations containing antigen peptides (20 μg), CpG (20 μg), and sonosensitizer (40 μg IR780) in 200 μl 10% sucrose. On days 11 and 16, ultrasound (1 MHz, 2 W/cm^2, 50% duty cycle, 5 min) was applied to the tumor region for selected groups. Bioluminescence from tumor cells was visualized using IVIS after intraperitoneal (i.p.) injection of luciferin. The body weights were monitored every two days. For a subset of experiments, animals were euthanized on day 20 and the major organs (heart, liver, spleen, lungs, and kidneys) were collected and fixed in 4% PFA. A series of 5-μm sections were stained with H&E before observation by a microscope (Nikon). To analyze the levels of CD8α$^+$ T cells in the tumor, tumors were harvested from animals on day 20, and the frequency of antigen-specific CD8α$^+$ T cells in the tumor was analyzed as described above. In some experiments, cured animals were rechallenged with 1×10^6 TC1-luc cells by intravenous injection on day 60. Age-matched naïve mice were used as the control group and intravenously injected with 1×10^6 TC1-luc cells. Tumor growth was monitored by using IVIS to measure the luciferase signal from tumor cells. Animals were euthanized when they had difficulty in breathing.

Therapeutic studies on B16F10 tumors

For therapeutic studies on B16F10 tumor-bearing mice, female C57BL/6 mice of age 6–8 weeks (Vital river) were inoculated with 2.5×10^5 B16F10 tumor cells on the right flank through subcutaneous injection on day 0. On days 9 and 14, tumor-bearing mice were intravenously injected with different formulations containing antigen peptides (20 μg), CpG (20 μg), and sonosensitizer (40 μg IR780) in 200 μl 10% sucrose. On days 10 and 15, ultrasound (1 MHz, 2 W/cm^2, 50% duty cycle, 5 min) was applied to the tumor region for selected groups. Tumor growth was monitored every 2 days, and the tumor volume was calculated using the following equation: tumor volume = length × width^2 × 0.52. Animals were euthanized when individual tumor sizes reached 15 mm in any dimensions or when animals exhibited severe weight loss or active ulceration. To analyze the levels of CD8α$^+$ T cells in the tumor, tumors were harvested from animals on day 17, and the frequency of antigen-specific IFN-γ$^+$CD8α$^+$ T cells in the tumor was analyzed as described above.

Statistical analysis

Sample sizes were chosen based on our preliminary data. Mice were randomly assigned to different treatment groups. The investigators were not blinded to the study. At least three experimental replicates were performed for statistics. Data were analyzed by one-way or two-way ANOVA, followed by Tukey's multiple comparisons post-test or log rank (Mantel–Cox) test with Prism 8.0 (GraphPad Software). *P* values less than 0.05 were considered statistically significant. All values are reported as means ± SEM with the indicated sample size in each figure legend. No samples were excluded from the analysis.

Reporting summary

Further information on research design is available in the Nature Portfolio Reporting Summary linked to this article.

Data availability

Data supporting the findings of this study are available within the article, Supplementary, Source data files or from the corresponding author on request. Source data are provided with this paper.

References

1. Zhang, Y. L. et al. Different subsets of tumor infiltrating lymphocytes correlate with NPC progression in different ways. *Mol. Cancer* **9**, 4 (2010).
2. Gajewski, T. F. The next hurdle in cancer immunotherapy: overcoming the non-T-cell-inflamed tumor microenvironment. *Semin Oncol.* **42**, 663–671 (2015).
3. de Jong, R. A. et al. Presence of tumor-infiltrating lymphocytes is an independent prognostic factor in type I and II endometrial cancer. *Gynecol. Oncol.* **114**, 105–110 (2009).
4. Hirayama, M. & Nishimura, Y. The present status and future prospects of peptide-based cancer vaccines. *Int. Immunol.* **28**, 319–328 (2016).

5. Moon, J. J. et al. Interbilayer-crosslinked multilamellar vesicles as synthetic vaccines for potent humoral and cellular immune responses. *Nat. Mater.* **10**, 243–251 (2011).
6. Liu, H. et al. Structure-based programming of lymph-node targeting in molecular vaccines. *Nature* **507**, 519–522 (2014).
7. Kuai, R., Ochyl, L. J., Bahjat, K. S., Schwendeman, A. & Moon, J. J. Designer vaccine nanodiscs for personalized cancer immunotherapy. *Nat. Mater.* **16**, 489–496 (2017).
8. Ott, P. A. et al. An immunogenic personal neoantigen vaccine for patients with melanoma. *Nature* **547**, 217–221 (2017).
9. Hu, Z. et al. Personal neoantigen vaccines induce persistent memory T cell responses and epitope spreading in patients with melanoma. *Nat. Med.* **27**, 515–525 (2021).
10. Trimble, C. L. et al. A phase I trial of a human papillomavirus DNA vaccine for HPV16+ cervical intraepithelial neoplasia 2/3. *Clin. Cancer Res.* **15**, 361–367 (2009).
11. Trimble, C. L., Peng, S., Thoburn, C., Kos, F. & Wu, T. C. Naturally occurring systemic immune responses to HPV antigens do not predict regression of CIN2/3. *Cancer Immunol. Immunother.* **59**, 799–803 (2010).
12. Barnes, T. A. & Amir, E. HYPE or HOPE: the prognostic value of infiltrating immune cells in cancer. *Br. J. Cancer* **117**, 451–460 (2017).
13. Shin, H. & Iwasaki, A. A vaccine strategy that protects against genital herpes by establishing local memory T cells. *Nature* **491**, 463–467 (2012).
14. Soong, R. S. et al. Toll-like receptor agonist imiquimod facilitates antigen-specific CD8+ T-cell accumulation in the genital tract leading to tumor control through IFNgamma. *Clin. Cancer Res.* **20**, 5456–5467 (2014).
15. Barboy, O. et al. Modeling T cell temporal response to cancer immunotherapy rationalizes development of combinatorial treatment protocols. *Nat. Cancer* **5**, 742–759 (2024).
16. Lewis, S. M., Williams, A. & Eisenbarth, S. C. Structure and function of the immune system in the spleen. *Sci. Immunol.* **4**, eaau6085 (2019).
17. Mebius, R. E. & Kraal, G. Structure and function of the spleen. *Nat. Rev. Immunol.* **5**, 606–616 (2005).
18. Kranz, L. M. et al. Systemic RNA delivery to dendritic cells exploits antiviral defence for cancer immunotherapy. *Nature* **534**, 396–401 (2016).
19. Cheng, Q. et al. Selective organ targeting (SORT) nanoparticles for tissue-specific mRNA delivery and CRISPR-Cas gene editing. *Nat. Nanotechnol.* **15**, 313–320 (2020).
20. Dilliard, S. A., Cheng, Q. & Siegwart, D. J. On the mechanism of tissue-specific mRNA delivery by selective organ targeting nanoparticles. *Proc. Natl. Acad. Sci. USA* **118**, e2109256118 (2021).
21. Kimura, S., Khalil, I. A., Elewa, Y. H. A. & Harashima, H. Novel lipid combination for delivery of plasmid DNA to immune cells in the spleen. *J. Control Release* **330**, 753–764 (2021).
22. Han, X. et al. Red blood cell-derived nanoerythrosome for antigen delivery with enhanced cancer immunotherapy. *Sci. Adv.* **5**, eaaw6870 (2019).
23. Huang, X. et al. The landscape of mRNA nanomedicine. *Nat. Med* **28**, 2273–2287 (2022).
24. Fucikova, J. et al. Detection of immunogenic cell death and its relevance for cancer therapy. *Cell Death Dis.* **11**, 1013 (2020).
25. Chen, G. Y. & Nunez, G. Sterile inflammation: sensing and reacting to damage. *Nat. Rev. Immunol.* **10**, 826–837 (2010).
26. Choi, V., Rajora, M. A. & Zheng, G. Activating drugs with sound: mechanisms behind sonodynamic therapy and the role of nanomedicine. *Bioconjug. Chem.* **31**, 967–989 (2020).
27. Simoes, S., Moreira, J. N., Fonseca, C., Duzgunes, N. & de Lima, M. C. On the formulation of pH-sensitive liposomes with long circulation times. *Adv. Drug Deliv. Rev.* **56**, 947–965 (2004).
28. Kopf, M., Abel, B., Gallimore, A., Carroll, M. & Bachmann, M. F. Complement component C3 promotes T-cell priming and lung migration to control acute influenza virus infection. *Nat. Med.* **8**, 373–378 (2002).
29. Bompard, J. et al. Membrane fluidity as a new means to selectively target cancer cells with fusogenic lipid carriers. *Langmuir* **36**, 5134–5144 (2020).
30. Cheniour, M., Gueyrard, D., Goekjian, P. G., Granjon, T. & Marcillat, O. A convenient and versatile synthesis of Laurdan-like fluorescent membrane probes: characterization of their fluorescence properties. *RSC Adv.* **6**, 5547–5557 (2016).
31. Fonseca, F., Pénicaud, C., Tymczyszyn, E. E., Gómez-Zavaglia, A. & Passot, S. Factors influencing the membrane fluidity and the impact on production of lactic acid bacteria starters. *Appl. Microbiol. Biotechnol.* **103**, 6867–6883 (2019).
32. Scheinpflug, K., Krylova, O. & Strahl, H. Measurement of cell membrane fluidity by Laurdan GP: fluorescence spectroscopy and microscopy. *Methods Mol. Biol.* **1520**, 159–174 (2017).
33. Francian, A. et al. Intratumoral delivery of antigen with complement C3-bound liposomes reduces tumor growth in mice. *Nanomedicine* **18**, 326–335 (2019).
34. Sallusto, F., Cella, M., Danieli, C. & Lanzavecchia, A. Dendritic cells use macropinocytosis and the mannose receptor to concentrate macromolecules in the major histocompatibility complex class II compartment: downregulation by cytokines and bacterial products. *J. Exp. Med.* **182**, 389–400 (1995).
35. Chen, Q. et al. Photothermal therapy promotes tumor infiltration and antitumor activity of CAR T cells. *Adv. Mater.* **31**, e1900192 (2019).
36. Yue, W. et al. Checkpoint blockade and nanosonosensitizer-augmented noninvasive sonodynamic therapy combination reduces tumour growth and metastases in mice. *Nat. Commun.* **10**, 2025 (2019).
37. Sandoval, F. et al. Mucosal imprinting of vaccine-induced CD8(+) T cells is crucial to inhibit the growth of mucosal tumors. *Sci. Transl. Med.* **5**, 172ra120 (2013).
38. Litzinger, D. C. & Huang, L. Amphipathic poly(ethylene glycol) 5000-stabilized dioleoylphosphatidylethanolamine liposomes accumulate in spleen. *Biochim. Biophys. Acta* **1127**, 249–254 (1992).
39. Tokatlian, T. et al. Innate immune recognition of glycans targets HIV nanoparticle immunogens to germinal centers. *Science* **363**, 649–654 (2019).
40. Mold, C. Effect of membrane phospholipids on activation of the alternative complement pathway. *J. Immunol.* **143**, 1663–1668 (1989).
41. Kullberg, M., Martinson, H., Mann, K. & Anchordoquy, T. J. Complement C3 mediated targeting of liposomes to granulocytic myeloid derived suppressor cells. *Nanomedicine* **11**, 1355–1363 (2015).
42. Guo, P. et al. Nanoparticle elasticity directs tumor uptake. *Nat. Commun.* **9**, 130 (2018).
43. Li, X. et al. Cancer immunotherapy based on image-guided STING activation by nucleotide nanocomplex-decorated ultrasound microbubbles. *Nat. Nanotechnol.* **17**, 891–899 (2022).
44. Wu, Y. et al. Control of the activity of CAR-T cells within tumours via focused ultrasound. *Nat. Biomed. Eng.* **5**, 1336–1347 (2021).
45. Li, X., Lovell, J. F., Yoon, J. & Chen, X. Clinical development and potential of photothermal and photodynamic therapies for cancer. *Nat. Rev. Clin. Oncol.* **17**, 657–674 (2020).
46. Charpentier, M., Spada, S., Van Nest, S. J. & Demaria, S. Radiation therapy-induced remodeling of the tumor immune microenvironment. *Semin. Cancer Biol.* **86**, 737–747 (2022).
47. Guo, S. et al. Radiation-induced tumor immune microenvironments and potential targets for combination therapy. *Signal Transduct. Target Ther.* **8**, 205 (2023).
48. Chang, M. C. et al. Irradiation enhances abscopal anti-tumor effects of antigen-specific immunotherapy through regulating tumor microenvironment. *Mol. Ther.* **26**, 404–419 (2018).

49. Chen, W. & Huang, L. Induction of cytotoxic T-lymphocytes and antitumor activity by a liposomal lipopeptide vaccine. *Mol. Pharm.* **5**, 464–471 (2008).
50. Zhu, W. et al. Sonodynamic therapy with immune modulatable two-dimensional coordination nanosheets for enhanced anti-tumor immunotherapy. *Nano Res.* **14**, 212–221 (2020).
51. Mastronarde, D. N. Automated electron microscope tomography using robust prediction of specimen movements. *J. Struct. Biol.* **152**, 36–51 (2005).
52. Zheng, S. Q. et al. MotionCor2: anisotropic correction of beam-induced motion for improved cryo-electron microscopy. *Nat. Methods* **14**, 331–332 (2017).
53. Qiu, M. et al. Lung-selective mRNA delivery of synthetic lipid nanoparticles for the treatment of pulmonary lymphangioleiomyomatosis. *Proc. Natl. Acad. Sci. USA* **119**, e2116271119 (2022).
54. Kim, M. et al. Engineered ionizable lipid nanoparticles for targeted delivery of RNA therapeutics into different types of cells in the liver. *Sci. Adv.* **7**, eabf4398 (2021).
55. Nomikou, N. et al. The effects of ultrasound and light on indocyanine-green-treated tumour cells and tissues. *ChemMedChem* **7**, 1465–1471 (2012).
56. Kuai, R. et al. Robust anti-tumor T cell response with efficient intratumoral infiltration by nanodisc cancer immunotherapy. *Adv. Ther.* **3**, 2000094 (2020).
57. Ochyl, L. J. & Moon, J. J. Whole-animal imaging and flow cytometric techniques for analysis of antigen-specific CD8+ T cell responses after nanoparticle vaccination. *J. Vis. Exp.* **29**, e52771 (2015).
58. Kuai, R. et al. Elimination of established tumors with nanodisc-based combination chemoimmunotherapy. *Sci. Adv.* **4**, eaao1736 (2018).
59. Savage, T. M. et al. Chemokines expressed by engineered bacteria recruit and orchestrate antitumor immunity. *Sci. Adv.* **9**, eadc9436 (2023).
60. Nam, J. et al. Chemo-photothermal therapy combination elicits anti-tumor immunity against advanced metastatic cancer. *Nat. Commun.* **9**, 1074 (2018).

Acknowledgements

The work was supported in part by grants from National Natural Science Foundation of China (82173751 to R.K.; 32241031 and 32171195 to S.L.), National Key Research and Development Program of China (2023YFC3403100 to R.K.), Tsinghua University Initiative Scientific Research Program (2023Z11DSZ001, 2024Z11DSZ001, and 2022Z11QYJ036 to R.K.), start-up packages from Tsinghua University to R.K., support from Tsinghua-Peking Center for Life Sciences to R.K., support from the Key Laboratory of Innovative Drug Research and Evaluation to R.K, and Tsinghua University Spring Breeze Fund to S.L. (2021Z99CFZ004). We acknowledge H. Peng (University of Chinese Academy of Sciences, Beijing) for the provision of MC38-OVA cells, X. Lin (Tsinghua University, Beijing) for MC38 cells and CD11c-DTR mice, and Y. Fu (Tsinghua University, Beijing) for *Batf3*$^{-/-}$ mice.

Author contributions

J.H. and R.K. designed the experiments. J.H., C.W., X.F., J.L, X.S. and H.L. performed the experiments. J.H. and R.K. analyzed the data. J.Z., C.P., and S.L. contributed to the cryo-electron microscopy (cryo-EM). J.M.K. contributed to data analysis and critically reviewing and editing the manuscript. J.H. and R.K. wrote the manuscript.

Competing interests

A patent application (2023100745723) has been filed based on the ultrasound-responsive liposomal nanovaccines for simultaneously programing the expansion and intratumoral infiltration of T cells, with R.K., J.H. and C.W. as inventors. J.M.K has been a paid consultant and or equity holder for companies (listed here: https://www.karplab.net/team/jeff-karp). J.M.K. is a paid consultant and holds equity in Corner Therapeutics, a company that has licensed IP generated by J.M.K. that may benefit financially if the IP is further validated. R.K. holds equity in Corner Therapeutics. The interests of J.M.K. were reviewed and are subject to a management plan overseen by his institutions in accordance with its conflict of interest policies. The remaining authors declare no competing interests.

Additional information

Supplementary information The online version contains supplementary material available at https://doi.org/10.1038/s41467-024-52104-z.

Correspondence and requests for materials should be addressed to Rui Kuai.

Peer review information *Nature Communications* thanks Francesca Cavalieri and the other, anonymous, reviewer(s) for their contribution to the peer review of this work. A peer review file is available.